RESEARCH ARTICLE | OCTOBER 07 2024

Simultaneous co-axial multi-modal inspection using a laser driven x-ray and neutron source

C. D. Armstrong ; G. G. Scott ; S. Richards ; K. Fedorov ; A. Laker-Illoul ; G. Hull ; J. K. Patel ; N. Booth ; R. Clarke ; P. P. Rajeev ; R. Simpson ; T. Ma ; C. Hernandez-Gomez

Rev. Sci. Instrum. 95, 103102 (2024)
https://doi.org/10.1063/5.0199999

Review of Scientific Instruments ARTICLE pubs.aip.org/aip/rsi

Simultaneous co-axial multi-modal inspection using a laser driven x-ray and neutron source

Cite as: Rev. Sci. Instrum. 95, 103102 (2024); doi: 10.1063/5.0199999
Submitted: 5 February 2024 • Accepted: 4 September 2024 •
Published Online: 7 October 2024

C. D. Armstrong,[1,a)] G. G. Scott,[1] S. Richards,[2] K. Fedorov,[1] A. Laker-Illoul,[1] G. Hull,[1] J. K. Patel,[1,3] N. Booth,[1] R. Clarke,[1] P. P. Rajeev,[1] R. Simpson,[4] T. Ma,[4] and C. Hernandez-Gomez[1]

AFFILIATIONS

[1] Central Laser Facility, Rutherford Appleton Laboratory, Harwell OX11 6FQ, United Kingdom
[2] STFC Technology, Rutherford Appleton Laboratory, Harwell OX11 6FQ, United Kingdom
[3] SUPA Department of Physics, University of Strathclyde, Glasgow G4 0NG, United Kingdom
[4] Lawrence Livermore National Laboratory, Livermore, California 94550, USA

[a)] Author to whom correspondence should be addressed: chris.armstrong@stfc.ac.uk

ABSTRACT

Laser-plasma interactions have been demonstrated to produce bright sources of energetic radiation including ions, electrons, photons across the electro-magnetic spectrum, and neutrons. Combinations of species can significantly increase information from non-destructive imaging. Here we demonstrate single-shot co-axial radiography with both x-ray and fast-neutron radiation from a laser-driven source using a pair of gated microchannel plate photomultiplier tube channels and a fast scintillator medium. The outlined system demonstrates recovery full-width-half-maximum of (18 ± 3) ns, which is sufficient to isolate x-rays from neutrons up to (72 ± 20) MeV and could be isolated only a short distance (2 m) from the target.

I. INTRODUCTION

High intensity laser plasma interactions can generate a wide variety of radiation, in terms of both species and energy, by tuning the plasma and laser conditions. The different radiation types share a common set of characteristics; they are short pulse (< ps),[1–3] emanate from a small source (100 nm–1 mm),[4–8] and can be tuned by subtle variations in the laser parameters or target.[9–13] There has been significant interest in developing these sources for radiography, with multiple groups demonstrating radiography with x-rays,[7,9,14,15] ions,[16–18] and neutrons.[19,20] Of note is recent work by Ostermayr *et al.*,[21] Gilbert *et al.*,[22] Yu *et al.*,[23] and Yogo *et al.*,[24] demonstrating the potential of multi-species radiographic inspection to determine more information for a given sample.

Due to the significant differences in attenuation cross-sections for x-rays and neutrons interacting with matter, there is interest in developing so called complementary inspection techniques, where a combination of radiation types is used to probe samples. To date, these examples have been limited to either orthogonal projections[21] or projections completed one after the other.[22] Achieving simultaneous radiography from a single projection angle but different radiation types would allow inspection of dynamic samples. Due to the ultra-short emission time of laser-driven sources at some distance from the interaction, the radiation will temporally disperse according to its velocity; photons therefore will reach detectors at a time $t_\gamma = t_0 + r/c$, where r is the distance to the detector and t_0 is the laser-interaction time, whereas massive particles will arrive at time $t_n = t_0 + r/\beta c$, where β is the normalized velocity depending on the particle's energy. With a sufficiently fast imaging system, it is therefore possible to separate the arrival of the photons and massive radiation species such as neutrons.

Herein we demonstrate a proof-of-principle multimodal imaging (MMI) detector scheme with initial experimental results to achieve simultaneous co-axial inspection of a sample with both fast neutrons and x-rays, driven from a single laser-plasma interaction. The article is structured as follows: a description of the diagnostic operating principle, experimental results from the Vulcan Laser at the Central Laser Facility with simulations supporting the results,

and a discussion on future applications for the scheme. The device outlined is similar in concept to the Neutron Imaging System (NIS) that is deployed on the National Ignition Facility[25] to detect neutron radiation from their interactions directly rather than as a means to produce a radiograph. The MMI detector design presented in this article has been developed to operate at distances significantly closer to target than the NIS.

II. MULTI-CHANNEL GATED IMAGING FOR RELATIVISTIC RADIATION DETECTION

A. Concept

Fast plastic scintillators, such as BC-422q or EJ-232q, report decay times at sub-nanosecond levels,[26,27] providing a method to isolate the arrival of photons and neutrons (t_γ and t_n). The temporal response of a scintillator-detector system is a convolution of the radiation pulse and the scintillator recovery, integrated with respect to the exposure length. Figure 1 shows how different cases appear from the perspective of a detector system. If we consider an ideal system where the scintillator recovery and the frame time are a delta function, we would be able to resolve any arbitrary radiation pulse—as shown in the bottom row of Fig. 1. However, if the scintillator has a decay constant, τ_s, and the frame is active for a finite time, τ_g, the resulting convolution can occlude features in the initial pulse. Any light incident on the sensor during the exposure is integrated into a single measurement. Therefore, for conventional cameras, the limit on temporal resolution is on the order of μs.[28–31] Gated MCPs, however, provide a way to narrow this window.[25,32] The temporal response for a gated MCP is as short as a few ns.[32,33]

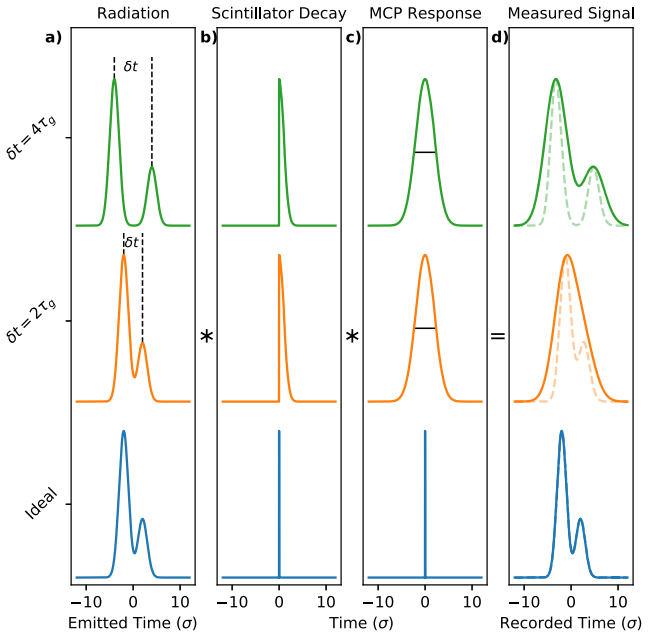

FIG. 1. A generalized view of the temporal response: (a) for any arbitrary radiation pulse, (d) the measured signal is the convolution of (b) the scintillator decay, and (c) the MCP response. When the separation between features in the radiation is larger than the MCP response window, we expect to be able to distinguish the features in the measurement. The dashed trace in the final column is the input radiation pulse to demonstrate the effect of the convolution. Throughout, the radiation pulses are Gaussian distributions with $\sigma = \tau_g/2$, the scintillator decay is a half-Gaussian with $\sigma = \tau_g/2$, and the MCP response is a Gaussian with $\sigma = \tau_g$.

The smallest resolvable temporal feature of a MCP-Scintillator system is limited to the combination of these features and can be expressed as $\tau_t \approx \sqrt{\tau_s^2 + \tau_{MCP}^2}$. For the design presented herein, we used a single 30 mm thick 300 × 300 mm^2 area BC-422q scintillator with a fast principle decay of $\tau_s \approx 1$ ns, imaged by two independently gated microchannel-plate (MCP) image intensifiers to provide the necessary isolation. The image intensifiers are Hamamatsu C9546-03[32] with a two stage MCP and a minimum gate time of $t_{MCP} \approx 3$ ns. Combined, this system has a fundamental limit, therefore, of $\tau \approx 3.1$ ns, and since we have independent control of the two MCP channels, we can equate this to an effective frame rate by

$$\nu' \approx 1/\sqrt{\tau_s^2 + \tau_{MCP}^2} \approx 300 \text{ MHz}. \quad (1)$$

Far exceeding current limits on existing single systems,[34] albeit only for two frames. To calculate what energies this minimum-time/frame-rate corresponds to, we need to evaluate $t_\gamma - t_n$ considering relativistic effects for energetic particles of some rest mass-energy E_0. We can express the separation in time at a position r from the source as a function of kinetic energy, E_k by

$$dt = t_\gamma - t_n(E) = \frac{r}{c}\left(1 - \sqrt{\frac{(E_k + E_0)^2}{E_k(2E_0 + E_k)}}\right). \quad (2)$$

This is evaluated in Fig. 2 for distances up to 100 m and neutron energies up to 100 MeV, demonstrating the requirement for

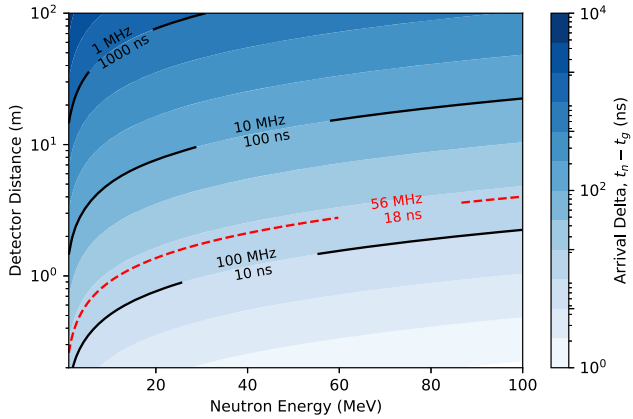

FIG. 2. Arrival time difference between energetic neutrons and the prompt x-ray flash emitted from a laser-plasma interaction as a function of distance and neutron energy. The solid lines indicate the limits on detection for 1, 10, and 100 MHz systems; the dashed line is the limit for the detector scheme espoused here with an effective frame rate of 56 MHz or an equivalent frame interval time of (18± 3) ns.

ultra-fast detector responses if we wish to isolate neutrons within a reasonable flight path. Regions above each solid line indicate which neutron energies and distances are resolvable for different effective temporal resolutions. The dashed line in Fig. 2 is the result of the system outlined in this article. We measured an effective gate-time (see Fig. 4 and surrounding discussion) of (18 ± 3) ns, which was sufficient to isolate the signals but larger than the fundamental limit in Eq. (1).

B. Implementation

We fielded this diagnostic on an experiment at the Vulcan Laser Facility. The experimental geometry is shown in Fig. 3. We used two separate picosecond lasers focused onto a (25 ± 5) μm deuterated-plastic (CD) target with a controlled delay between their arrival. A "pre-conditioning" pulse of (50 ± 2.8) J in (1 ± 0.3) ps was focused to a 30 μm diameter spot to pre-expand the CD target.[35] The main driving laser arrived up to 150 ps later and delivered (180 ± 25) J in (29 ± 2) ps to a focal spot of (5.4 ± 1.2) μm. In doing so, we accelerate a high population of relativistic electrons into the target. These in turn generate bremsstrahlung radiation and, as they escape the target, establish a TV/m electrostatic sheath field that ionizes and accelerates ions, known as Target Normal Sheath Acceleration.[36] This ion emission (deuterons and protons) from the CD target was directed onto a 2 mm lithium slab 75 mm from the interaction in a pitcher-catcher style geometry.[37] We used a half-height slab of lithium [indicated in Fig. 3(a)] to permit on-shot characterization of the ion emission from the target via a Thomson parabola positioned normal to the rear of the target 1 m from the interaction. The neutron spectrum was characterized at 0°, 10°, and 45° relative to target normal using neutron time-of-flight (nTOF) scintillators and photo-multiplier tubes (PMTs) at distances >3 m.

The MMI was positioned 2 m from the target at 12°–20° relative to target normal such that we can infer the incident neutron spectra on the detector with the signal from the nTOF detectors. The MMI scintillator emission is collected by a lens and relayed to the image intensifiers and camera system at a working distance of 840 mm. Two cameras are offset from the central axis by 4° in opposite directions. Without reflective cavities, the variation in emission profile over a small angle has been demonstrated to be *quasi*-isotropic.[38] Therefore, the angular offset between each camera causes a negligible difference in the sensitivity of the system.

III. EXPERIMENTAL DEMONSTRATION

The trigger timing for both the x-ray (C_X) and neutron (C_N) channels on the MMI diagnostic is crucial to operation. For the initial calibration/characterization shots of the experiment, we positioned a photo-diode at the scintillator plane and recorded the relative time of arrival of the optical laser flash to estimate the trigger delay required for the MMI. A minimum gate window of $\tau_{MCP} = 7$ ns was used during the experiment to minimize the effect of jitter in our timing system. On subsequent shots, we were able to time C_X and C_N on the MMI to the peak of the x-ray emission, at which point we fixed the timing of C_X and continued to vary C_N. In Fig. 4, we show the effect of varying the C_N central gate time relative to the C_X. The signal on each camera has been integrated over all pixels to avoid the effects of hot-spots and is shown relative to each other to mitigate the varying flux levels we experienced on the experiment. Interestingly, this resultant x-ray peak width is longer than expected. The x-ray source from a laser-driven pulse is expected to be on the order of the driving laser pulse ~ pico-seconds, which is

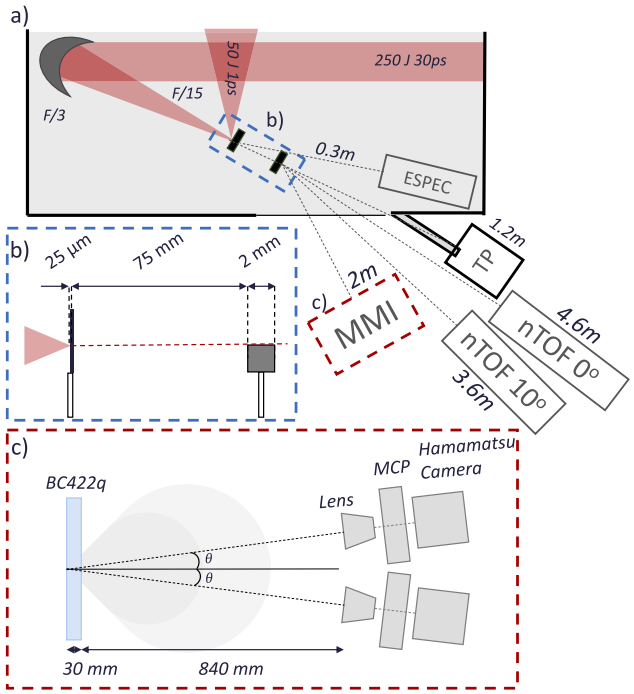

FIG. 3. Schematics of the (a) experimental geometry, (b) multi-modal imager geometry, and (c) target setup. In the figure, nTOF refers to neutron time-of-flight; MMI is the multi-modal-imager diagnostic discussed in this paper.

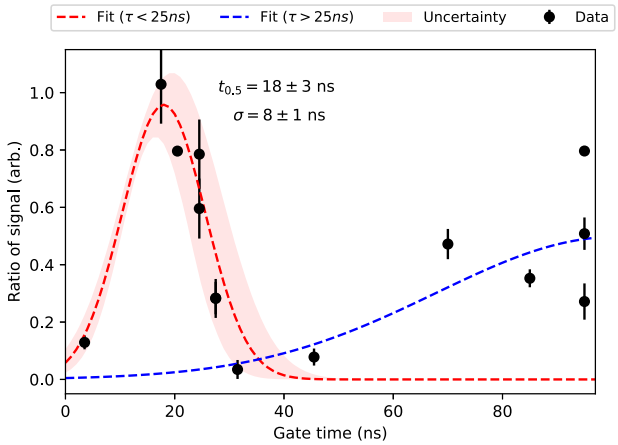

FIG. 4. Ratio of the integrated signal on each channel, where the gate-center for C_N was varied with respect to the driving laser pulse and C_X was fixed. The red dashed line is a Gaussian fit to the effective x-ray response of the two channel system, indicating a FWHM = (18 ± 3) ns, and the blue dashed line indicates a Gaussian fit to the neutron signal.

effectively a delta function in comparison to τ_{MCP}. Instead, a fitted Gaussian to the measured data demonstrates a FWHM of the x-ray component is equal to $\tau_{MMI} = (18 \pm 3)$ ns, $\sim 2.3 \times \tau_{MCP}$, suggesting that either the minimum gate-time is indicative of the rising-/falling-edge of the MCP response rather than the full width (and is therefore effectively double) or the jitter of the timing system is higher than expected. Regardless of the exact reason for the extended duration, this τ_{MMI} is sufficient to isolate the neutron and x-ray signal, as demonstrated by subsequent data points in Fig. 5. The camera signal begins to rise again as the neutrons are arriving at the detector. The onset of the second signal is related to the peak energy and distribution of the neutrons from the same shot—hence the increased scatter—and suggest a peak neutron energy of ~40 MeV. While we did not extend the delay scan out further, we would expect the signal to decay as the lower energy (and slower) neutron distribution passes.

To demonstrate the imaging capability of the MMI, we positioned a 5 mm sheet of Pb in contact with the scintillator. This material and thickness were chosen to maximize the attenuation in the x-ray emission while transmitting the neutron spectrum. We see exactly the result in Fig. 5, where we can clearly see a shadow from the Pb sheet on the x-ray image, but 50 ns later on the neutron channel, we see an almost uniform profile. This is shown alongside an earlier shot when the neutron channel was set to 20 ns before the shot to demonstrate that the signal in both channels is significantly above background. The plots below the images show nTOF traces from the same shots, with the shaded regions indicating the MMI gate-window used to capture the respective images. Each image has been binned to 8×8 to reduce the effective noise. Of note here is that the x-ray signal is sufficient for the radiograph despite using a low-z target.

IV. DISCUSSION

We verified the signal recorded on the MMI diagnostic by simulating the results in Geant4.[40] The incident neutron energies were taken from the nTOF measurement closest to the MMI axis, with the measured light yield converted back to the relative neutron population via the method outlined in Ref. 39. The expected x-ray distribution, as measured on prior experiments using the Vulcan laser,[4] and the measured neutron distribution are shown in Fig. 6(a). Each radiation type was injected into the simulation over a $100 \times 100\,mm^2$ area incident onto a $20 \times 50 \times 5$ mm Pb sheet in front of a $100 \times 100 \times 30\ mm^3$ scintillator slab. The detector volume was split into $1 \times 1 \times 30\ mm^3$ voxels, and the energy deposited in each volume was recorded and shown as an image in Figs. 6(b) and 6(c). We used an exponential energy distribution for each radiation type with an effective temperature as shown in Fig. 6(a). We see immediate similarity to the experimental results where only the x-ray channel records the shadow of the Pb sheet, confirming the idea that we are able to independently resolve x-ray and neutron radiographs.

The results expressed here, while successful, demonstrate that single shot inspection with laser-driven neutrons is still a challenge. To achieve higher signal-to-noise images, we have a few options to improve this concept. First, the BC-422q scintillator used in this work uses quenching effects to reduce the decay time from 1.4 to

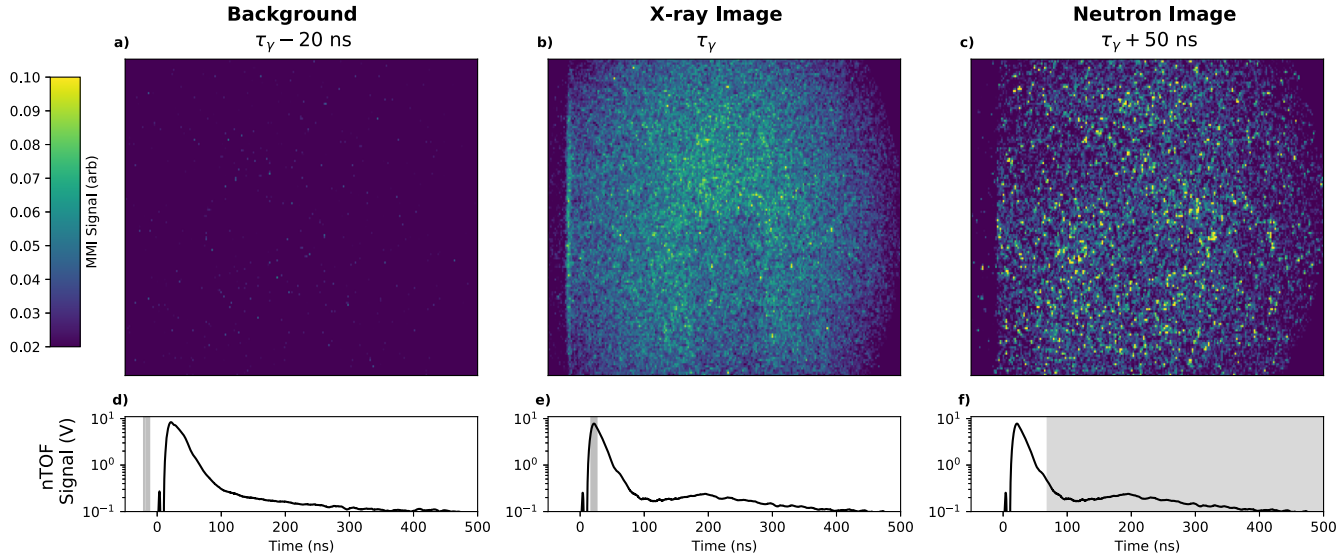

FIG. 5. Signal on the MMI device from three distinct time steps with the neutron time-of-flight (nTOF) trace from the same shot. Panels (a) and (d) are from a prior shot where the MMI channel was set to trigger before the interaction to demonstrate the background level on the MMI system. (b) and (c) and (e) and (f) are images from the same shot with the MMI set to receive the x-ray flash and the delayed neutron signal. Shaded regions on the nTOF trace indicate the temporal windows the MMI channels are set to receive. While the neutron window appears to be clipping the decay of the x-ray, it should be noted that the nTOF response is longer[39] than the MMI. Panels (a) and (d) were recorded on a separate shot to (b) and (c) and (e) and (f), hence the distinct nTOF traces.

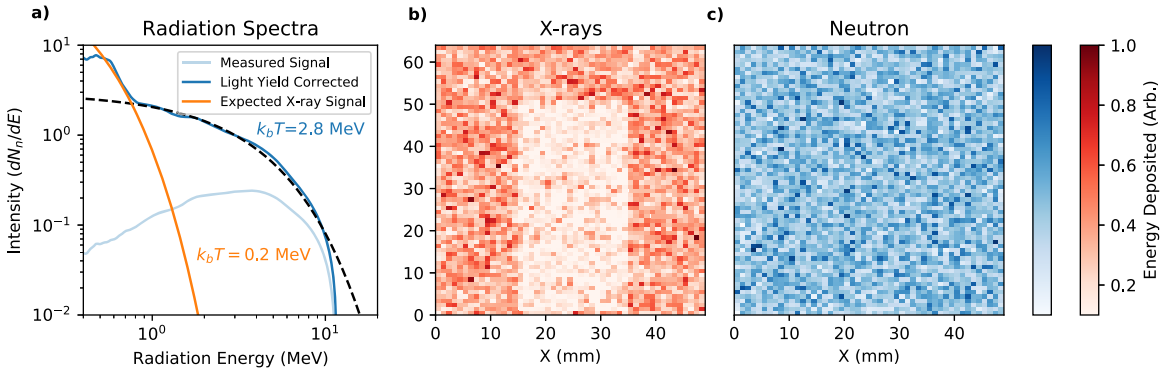

FIG. 6. (a) Measured neutron spectra from the same shot as Fig. 5, with expected x-ray spectra from laser intensity parameters.[4] Simulated radiograph for (b) x-rays and (c) neutrons matching the spectral conditions in panel (a), 2.8 MeV exponential distribution for neutrons, and a 200 keV exponential distribution for x-rays.

0.7 ns.[27] However, this also reduces the light yield by (3–4)×. Given the effective gate time measured in Sec. III is significantly greater than this, we can increase the detected optical signal on both cameras by using the un-quenched BC-422 scintillator. Second, we can improve the lens system by increasing the numerical aperture to capture more emission from the scintillator.[41] When altering the lens system, it would also be beneficial to introduce a mirror and shield the MCP and camera to minimize direct hits. These improvements to the efficiency of the system can only work to a point; the best method would be to increase the yield from the source itself. Neutron emission from laser-driven sources continues to increase in maximum yield, with recent work by Ren *et al.*[42] demonstrating a significant increase in neutron emission using a curved CD capsule and driving a fusion-like reaction. Deuteron-induced neutron generation has been demonstrated to produce a beam-like source of neutrons.[43] While this mechanism currently yields a lower total number of neutrons, the intensity of a beam-like emission could result in a significant increase in imaging quality. As demonstrated by Figs. 4 and 5, there is sufficient light in the neutron line to make multiple measurements at distinct times. By changing the gate time for the neutron camera, we are also changing the neutron energy and, more crucially, the arrival time of said neutrons at the sample. With increased signal, either from improvements to the diagnostic, source yield, or both, we can envision truly dynamic inspection of samples.

V. CONCLUSION

Herein we outline and demonstrate a concept for simultaneous co-axial multi-modal imaging with x-rays and neutrons driven by a high power laser interaction. The results show clear temporal separation between the radiation species and agree well with Monte-Carlo simulations of the resultant radiograph. While the signal-to-noise was low in this proof-of-principle demonstration, we outline methods to improve the detector system and, with further increases in neutron yield from laser-driven sources, we expect this to be a key application of future facilities. We also discuss how the technique can be expanded to multi-color neutron inspection of materials or ultra-fast dynamic inspection using the separation time of neutron energies at the sample plane.

ACKNOWLEDGMENTS

This research was supported by the UK Strategic Priorities Fund.

This work was performed under the auspices of the U.S. Department of Energy by the Lawrence Livermore National Laboratory under Contract Nos. DE-AC52-07NA27344 and DOE FES Measurements Innovations grant SCW1720 and with funding support from the Laboratory Directed Research and Development Program under tracking codes Grant Nos. 20-ERD-048 and 21-ERD-015. This document was prepared as an account of work sponsored by an agency of the United States government. Neither the United States government nor Lawrence Livermore National Security, LLC, nor any of their employees makes any warranty, expressed or implied, or assumes any legal liability or responsibility for the accuracy, completeness, or usefulness of any information, apparatus, product, or process disclosed, or represents that its use would not infringe privately owned rights. Reference herein to any specific commercial product, process, or service by trade name, trademark, manufacturer, or otherwise does not necessarily constitute or imply its endorsement, recommendation, or favoring by the United States government or Lawrence Livermore National Security, LLC. The views and opinions of authors expressed herein do not necessarily state or reflect those of the United States government or Lawrence Livermore National Security, LLC, and shall not be used for advertising or product endorsement purposes.

AUTHOR DECLARATIONS

Conflict of Interest

The authors have no conflicts to disclose.

Author Contributions

C. D. Armstrong: Conceptualization (lead); Formal analysis (lead); Investigation (lead); Methodology (lead); Writing – original draft (lead); Writing – review & editing (lead). **G. G. Scott**: Conceptualization (equal); Methodology (equal); Writing – review & editing (equal). **S. Richards**: Methodology (equal); Writing – review & editing (equal). **K. Fedorov**: Formal analysis (supporting); Writing – review & editing (supporting). **A. Laker-Illoul**: Investigation (supporting). **G. Hull**: Investigation (supporting). **J. K. Patel**: Formal analysis (supporting); Writing – review & editing (supporting). **N. Booth**: Investigation (supporting); Methodology (supporting); Project administration (supporting). **R. Clarke**: Funding acquisition (equal); Project administration (equal); Resources (equal); Supervision (equal); Writing – review & editing (supporting). **P. P. Rajeev**: Supervision (equal). **R. Simpson**: Investigation (supporting); Methodology (supporting). **T. Ma**: Supervision (supporting). **C. Hernandez-Gomez**: Funding acquisition (equal); Supervision (lead).

DATA AVAILABILITY

The original contributions presented in the study are publicly available. This data can be found here: https://edata.stfc.ac.uk/handle/.

APPENDIX: ON USE IN HIGH BACKGROUND ENVIRONMENTS

Continuous sources, such as AmBe sealed sources or DD/DT generators, typically utilize on pulse-shape discrimination (PSD), pulse height discrimination, or rely on low sensitivity to X-rays to isolate neutron/gamma information. They require measurement of individual interactions, which necessitate long duration measurement for sufficient statistics. In high background or highly scattering environments, it can be difficult to use PSD or absorption discrimination to differentiate between background sources and the imaging source.[44] The short pulse duration of a laser-driven source and the narrow gate-time of the MCP provide a unique distinction between the different species that is otherwise not possible to achieve. Since the respective sensitivity windows are only active for a short time in the MMI diagnostic presented here, there is a minimal impact from the background source.

REFERENCES

[1] H. Hamster, A. Sullivan, S. Gordon, W. White, and R. Falcone, "Subpicosecond, electromagnetic pulses from intense laser-plasma interaction," Phys. Rev. Lett. **71**, 2725 (1993).

[2] D. Jaroszynski, R. Bingham, E. Brunetti, B. Ersfeld, J. Gallacher, B. van Der Geer, R. Issac, S. Jamison, D. Jones, M. De Loos *et al.*, "Radiation sources based on laser–plasma interactions," Philos. Trans. R. Soc., A **364**, 689–710 (2006).

[3] A. Khachatryan, F. Van Goor, K.-J. Boller, A. Reitsma, and D. Jaroszynski, "Extremely short relativistic-electron-bunch generation in the laser wakefield via novel bunch injection scheme," Phys. Rev. Spec. Top.–Accel. Beams **7**, 121301 (2004).

[4] C. Armstrong, C. Brenner, C. Jones, D. Rusby, Z. Davidson, Y. Zhang, J. Wragg, S. Richards, C. Spindloe, P. Oliveira *et al.*, "Bremsstrahlung emission from high power laser interactions with constrained targets for industrial radiography," High Power Laser Sci. Eng. **7**, e24 (2019).

[5] A. Pirozhkov, T. Z. Esirkepov, T. Pikuz, A. Y. Faenov, K. Ogura, Y. Hayashi, H. Kotaki, E. Ragozin, D. Neely, H. Kiriyama *et al.*, "Burst intensification by singularity emitting radiation in multi-stream flows," Sci. Rep. **7**, 17968 (2017).

[6] H. S. Park, B. R. Maddox, E. Giraldez, S. P. Hatchett, L. T. Hudson, N. Izumi, M. H. Key, S. Le Pape, A. J. MacKinnon, A. G. MacPhee, P. K. Patel, T. W. Phillips, B. A. Remington, J. F. Seely, R. Tommasini, R. Town, J. Workman, and E. Brambrink, "High-resolution 17–75keV backlighters for high energy density experiments," Phys. Plasmas **15**, 072705 (2008).

[7] J.-N. Gruse, M. Streeter, C. Thornton, C. Armstrong, C. Baird, N. Bourgeois, S. Cipiccia, O. Finlay, C. Gregory, Y. Katzir *et al.*, "Application of compact laser-driven accelerator x-ray sources for industrial imaging," Nucl. Instrum. Methods Phys. Res., Sect. A **983**, 164369 (2020).

[8] A. Köhler, J. Couperus, O. Zarini, A. Jochmann, A. Irman, and U. Schramm, "Single-shot betatron source size measurement from a laser-wakefield accelerator," Nucl. Instrum. Methods Phys. Res., Sect. A **829**, 265–269 (2016).

[9] F. Albert and A. G. Thomas, "Applications of laser wakefield accelerator-based light sources," Plasma Phys. Controlled Fusion **58**, 103001 (2016).

[10] C. Armstrong, C. Brenner, E. Zemaityte, G. Scott, D. Rusby, G. Liao, H. Liu, Y. Li, Z. Zhang, Y. Zhang *et al.*, "Bremsstrahlung emission profile from intense laser-solid interactions as a function of laser focal spot size," Plasma Phys. Controlled Fusion **61**, 034001 (2019).

[11] J. Wood, "Betatron radiation from laser wakefield accelerators and its applications," Ph.D. thesis, Imperial College London, 2017.

[12] C. Underwood, C. Baird, C. Murphy, C. Armstrong, C. Thornton, O. Finlay, M. Streeter, M. Selwood, N. Brierley, S. Cipiccia *et al.*, "Development of control mechanisms for a laser wakefield accelerator-driven bremsstrahlung x-ray source for advanced radiographic imaging," Plasma Phys. Controlled Fusion **62**, 124002 (2020).

[13] O. Finlay, J. Gruse, C. Thornton, R. Allott, C. D. Armstrong, C. D. Baird, N. Bourgeois, C. Brenner *et al.*, "Characterisation of a laser plasma betatron source for high resolution x-ray imaging," Plasma Phys. Controlled Fusion **63**, 084010 (2021).

[14] J. Cole, J. Wood, N. Lopes, K. Poder, R. Abel, S. Alatabi, J. Bryant, A. Jin, S. Kneip, K. Mecseki *et al.*, "Tomography of human trabecular bone with a laser-wakefield driven x-ray source," Plasma Phys. Controlled Fusion **58**, 014008 (2015).

[15] C. Brenner, S. Mirfayzi, D. Rusby, C. Armstrong, A. Alejo, L. Wilson, R. Clarke, H. Ahmed, N. Butler, D. Haddock *et al.*, "Laser-driven x-ray and neutron source development for industrial applications of plasma accelerators," Plasma Phys. Controlled Fusion **58**, 014039 (2015).

[16] G. Sarri, C. Cecchetti, L. Romagnani, C. Brown, D. Hoarty, S. James, J. Morton, M. E. Dieckmann, R. Jung, O. Willi *et al.*, "The application of laser-driven proton beams to the radiography of intense laser–Hohlraum interactions," New J. Phys. **12**, 045006 (2010).

[17] H. Ahmed, M. E. Dieckmann, L. Romagnani, D. Doria, G. Sarri, M. Cerchez, E. Ianni, I. Kourakis, A. L. Giesecke, M. Notley *et al.*, "Time-resolved characterization of the formation of a collisionless shock," Phys. Rev. Lett. **110**, 205001 (2013).

[18] A. Mackinnon, P. Patel, M. Borghesi, R. Clarke, R. Freeman, H. Habara, S. Hatchett, D. Hey, D. Hicks, S. Kar *et al.*, "Proton radiography of a laser-driven implosion," Phys. Rev. Lett. **97**, 045001 (2006).

[19] K. Lancaster, S. Karsch, H. Habara, F. Beg, E. Clark, R. Freeman, M. Key, J. King, R. Kodama, K. Krushelnick *et al.*, "Characterization of Li7(p,n)7Be neutron yields from laser produced ion beams for fast neutron radiography," Phys.Plasmas **11**, 3404–3408 (2004).

[20] N. Guler, P. Volegov, A. Favalli, F. E. Merrill, K. Falk, D. Jung, J. L. Tybo, C. H. Wilde, S. Croft, C. Danly *et al.*, "Neutron imaging with the short-pulse laser driven neutron source at the trident laser facility," J. Appl. Phys. **120**, 154901 (2016).

[21] T. Ostermayr, C. Kreuzer, F. Englbrecht, J. Gebhard, J. Hartmann, A. Huebl, D. Haffa, P. Hilz, K. Parodi, J. Wenz *et al.*, "Laser-driven x-ray and proton micro-source and application to simultaneous single-shot bi-modal radiographic imaging," Nat. Commun. **11**, 6174 (2020).

[22] A. J. Gilbert, B. S. McDonald, and M. R. Deinert, "Advanced algorithms for radiographic material discrimination and inspection system design," Nucl. Instrum. Methods Phys. Res., Sect. B **385**, 51–58 (2016).

[23] Y. Yu, R. Zhang, L. Lu, and Y. Yang, "The bimodal neutron and x-ray imaging driven by a single electron linear accelerator," Appl. Sci. **11**, 6050 (2021).

[24]A. Yogo, S. R. Mirfayzi, Y. Arikawa, Y. Abe, T. Wei, T. Mori, Z. Lan, Y. Hoonoki, D. O. Golovin, K. Koga *et al.*, "Single shot radiography by a bright source of laser-driven thermal neutrons and x-rays," Appl. Phys. Express **14**, 106001 (2021).
[25]F. Merrill, D. Bower, R. Buckles, D. Clark, C. Danly, O. Drury, J. Dzenitis, V. Fatherley, D. Fittinghoff, R. Gallegos *et al.*, "The neutron imaging diagnostic at NIF (invited)," Rev. Sci. Instrum. **83**, 10D317 (2012).
[26]M. Hamel, "Progress in fast and red plastic scintillators," Chemosensors **10**, 86 (2022).
[27]Luxium Plastic Scintillator Datasheets, 2022, available at, https://www.luxiumsolutions.com/radiation-detection-scintillators/plastic-scintillators/fast-timing-bc-418-bc-420-bc-422-bc-422q (accessed 29 11 2023).
[28]T4040 Series Datasheet, 2022, available at, https://www.phantomhighspeed.com/products/cameras/tseries/t4040 (accessed 29 11 2023).
[29]i-SPEED 7 Series Datasheet, 2022, available at, https://www.ix-cameras.com/downloads/i-SPEED_7_Series_Datasheet.pdf (accessed 29 11 2023).
[30]L. Jones, S. Bell, B. Cline, T. Gardiner, M. Hart, M. Prydderch, P. Seller, M. Veale, and M. Wilson, "Spectroscopic X-ray imaging at MHz frame rates—The HEXITEC$_{MHz}$ ASIC," J. Instrum. **17**, C10012 (2022).
[31]J. Zhang, M. Andrä, R. Barten, A. Bergamaschi, M. Brückner, S. Chiriotti-Alvarez, R. Dinapoli, E. Fröjdh, D. Greiffenberg, P. Kozlowski *et al.*, "Design and first tests of the Gotthard-II readout asic for the european x-ray free-electron laser," J. Instrum. **16**, P04015 (2021).
[32]C9546-03 - Datasheet, 2022, available at, https://www.hamamatsu.com/content/dam/hamamatsu-photonics/sites/documents/99_SALES_LIBRARY/etd/II_TII0007E.pdf (accessed 29 11 2023).
[33]GM-MCP - Gate Module Datasheet, 2007, available at.https://www.photek.com/pdf/datasheets/electronics/GM-MCP.pdf (accessed 31 07 2024).
[34]T. G. Etoh, A. Q. Nguyen, Y. Kamakura, K. Shimonomura, T. Y. Le, and N. Mori, "The theoretical highest frame rate of silicon image sensors," Sensors **17**, 483 (2017).
[35]P. McKenna, D. Carroll, O. Lundh, F. Nürnberg, K. Markey, S. Bandyopadhyay, D. Batani, R. Evans, R. Jafer, S. Kar *et al.*, "Effects of front surface plasma expansion on proton acceleration in ultraintense laser irradiation of foil targets," Laser Part. Beams **26**, 591–596 (2008).
[36]M. Passoni, L. Bertagna, and A. Zani, "Target normal sheath acceleration: Theory, comparison with experiments and future perspectives," New J. Phys. **12**, 045012 (2010).
[37]L. Willingale, G. Petrov, A. Maksimchuk, J. Davis, R. Freeman, A. Joglekar, T. Matsuoka, C. Murphy, V. Ovchinnikov, A. Thomas *et al.*, "Comparison of bulk and pitcher-catcher targets for laser-driven neutron production," Phys. Plasmas **18**, 083106 (2011).
[38]J. K. Patel, D. Neely, C. D. Armstrong, and R. J. Clarke, "Improving collimation of optical flux emission from scintillator crystals," in *CLF Annual Report 2020* (Science & Technology Facilities Council, Rutherford Appleton Laboratory, Didcot, UK, 2020), https://www.clf.stfc.ac.uk/gallery/40-Patel.pdf.
[39]S. Mirfayzi, S. Kar, H. Ahmed, A. Krygier, A. Green, A. Alejo, R. Clarke, R. Freeman, J. Fuchs, D. Jung *et al.*, "Calibration of time of flight detectors using laser-driven neutron source," Rev. Sci. Instrum. **86**, 073308 (2015).
[40]J. Allison, K. Amako, J. Apostolakis, P. Arce, M. Asai, T. Aso, E. Bagli, A. Bagulya, S. Banerjee, G. Barrand *et al.*, "Recent developments in geant4," Nucl. Instrum. Methods Phys. Res., Sect. A **835**, 186–225 (2016).
[41]C. D. Armstrong, G. Scott, S. Richards, J. Patel, K. Fedorov, R. Gray, K. Welsby, and P. P. Rajeev, "X-ray detector requirements for laser-plasma accelerators," Front. Phys. **11**, 1286442 (2023).
[42]G. Ren, J. Yan, J. Liu, K. Lan, Y. Chen, W. Huo, Z. Fan, X. Zhang, J. Zheng, Z. Chen *et al.*, "Neutron generation by laser-driven spherically convergent plasma fusion," Phys. Rev. Lett. **118**, 165001 (2017).
[43]A. Alejo, A. Krygier, H. Ahmed, J. Morrison, R. Clarke, J. Fuchs, A. Green, J. Green, D. Jung, A. Kleinschmidt *et al.*, "High flux, beamed neutron sources employing deuteron-rich ion beams from D_2O-ice layered targets," Plasma Phys. Controlled Fusion **59**, 064004 (2017).
[44]Y.-H. He, Y.-Y. Huang, Z.-R. Zeng, Y.-F. Li, J.-H. Tan, L.-M. Chen, L.-A. Wu, M.-F. Li, B.-G. Quan, S.-L. Wang, and T. J. Liang, "Single-pixel imaging with neutrons," Sci. Bull. **66**, 133–138 (2021).